

## ORGANIC SYNTHESIS

# Excision of organic macrocycles from covalent organic frameworks

Roberto Sánchez-Naya<sup>1,2</sup>, Juan Pablo Cavalieri<sup>1,2,3</sup>, Jorge Albalad<sup>1,2\*</sup>, Alba Cortés-Martínez<sup>1,2</sup>, Kaiyu Wang<sup>4,5</sup>, Carles Fuertes-Espinosa<sup>6</sup>, Teodor Parella<sup>7</sup>, Sara Fiori<sup>1</sup>, Esteve Ribas<sup>1</sup>, Aitor Mugarza<sup>1,8</sup>, Xavi Ribas<sup>6</sup>, Jordi Faraudo<sup>9</sup>, Omar M. Yaghi<sup>4,5</sup>, Inhar Imaz<sup>1,2\*</sup>, Daniel MasPOCH<sup>1,2,8\*</sup>

Molecules are typically synthesized through stepwise processes involving chemical reactions between simple molecular precursors. Here, we report an advance in the synthesis of new organic molecules based on the approach of clip-off chemistry, in which molecules are excised from ordered, extended organic structures. We synthesized macrocycles by selectively cleaving them out of covalent organic frameworks. The synthesized macrocycles include eight macrocyclic polyamides with 114-, 138-, and 162-atom rings, and one 114-atom ring macrocyclic polyimide. This excision approach expands the scope of chemical organic synthesis to previously inaccessible macromolecules.

The synthesis of new organic molecules is usually approached through stepwise processes that involve reactions between simpler precursors (1–7). However, a crystalline solid can be viewed as preformed template from which molecules, such as clusters and cages, can be excised through specific cleavage reactions. The original concept of excision in synthesis was first introduced in the isolation of unusual clusters from inorganic solids (8). We recently extended this concept and demonstrated its success in molecular structures, enabling the synthesis of metal-organic clusters and cages from metal-organic frameworks through “clip-off chemistry” (9–11).

We extended this approach to another demanding synthesis: organic macrocyclic molecules. Challenges in the synthesis of these molecules include low selectivity, poor yields given the increasing difficulty of directing the closure of larger rings, and the need for complex purification steps (12–21), as well as stringent control to avoid side products such as linear oligomers or smaller rings. We show that macrocycles can be synthesized with precision and in high yields through their excision from covalent organic frameworks (COFs) (Fig. 1) (22–25), which can be disassembled not into their original building blocks but into larger macrocycles (26–29). Specifically, we synthesized hexagonal polyamide- and polyimide-linked macrocycles. Moreover, we demonstrate that our excision synthesis strategy can be coupled with isorecticular chemistry to rationally tune both the size and functionality of the synthesized macrocycles, enabling the synthesis of macrocycles with progressively larger ring sizes, including 114-, 138- and 162-atom rings, as well as the incorporation of functional groups such as fluorine.

## Design and synthesis of COFs for their conversion to unusual macrocycles

The synthesis of organic macrocycles by excision requires an appropriate topology of the COF precursor. A parent framework would need to contain at least two distinct types of pores. One would correspond to our product and should not contain cleavable bonds. Adjacent pores would contain cleavable bonds that would liberate our target macrocycle. In the case that we report here, the cleavable bonds are olefinic bonds and the cleavage method is ozonolysis. This design ensures that, upon exposure to ozone, every cleavable bond breaks, releasing the first targeted pores as discrete macrocycles.

After exploring two-dimensional (2D) COFs that would satisfy our requirements, we chose those with an underlying Kagome (kgm) topology (30–33). These kgm COFs are typically constructed by combining a planar tetratopic ( $D_{4h}$ ,  $D_{2h}$ ,  $C_{2h}$ ) organic building block with a linear one, resulting in a 2D lattice comprising a periodic arrangement of alternating hexagonal and triangular pores (Fig. 1). Closer analysis of the structure reveals that the hexagonal pores are exclusively extended by the condensation linkages formed during COF synthesis, and these are interconnected by the bisection of the tetratopic building blocks. Thus, we envisioned that by incorporating cleavable olefinic bonds into the central part of this later linker, the cleavable bonds would only be located within the triangular pores and that, once cleaved, the hexagonal pores (our desired macrocycles), would be liberated for isolation.

Following the aforementioned design, we began by synthesizing a 2D iminic kgm COF (hereafter, im-COF-1) by reacting the olefinic-containing (*E*)-3,3',5,5'-tetrakis(4-aminophenyl)stilbene [(StTA)  $C_{2h}$  building block] and terephthalaldehyde [(PDA) linear building block] in a scintillation vial for 3 days at 85°C, using benzoic acid as a catalyst and aniline as a structural modulator [see supplementary materials (SM) for detailed synthetic protocol and fig. S1] (34). Powder x-ray diffraction (PXRD) measurements of the resulting powder revealed sharp, intense peaks at 2.21°, 3.75°, 4.29°, 5.67°, and 7.64° (fig. S2). A full-profile Pawley fitting based on this model gave final unit cell parameters of  $a = b = 49.33$  Å and  $c = 3.53$  Å, with angles of  $\alpha = \beta = 90^\circ$  and  $\gamma = 120^\circ$ , and good agreement factors ( $R_p = 2.3\%$  and  $R_{wp} = 4.3\%$ , figs. S3 and S4). The simulated PXRD pattern using these cell parameters matched well with the experimental pattern of the kgm lattice, confirming the successful synthesis of im-COF-1.

Further evidence of iminic COF formation was provided by Fourier transformance infrared (FTIR) spectroscopy and  $^{13}C$  cross polarization-magic angle spinning (CP-MAS) solid-state nuclear magnetic resonance (NMR). The FTIR spectrum showed the characteristic imine-stretching band at 1620  $cm^{-1}$  (fig. S5), whereas the  $^{13}C$  CP-MAS NMR spectrum exhibited the corresponding imine peak at 157.7 parts per million (ppm) (fig. S6). Finally, porosity was measured using nitrogen-physisorption isotherms at 77 K, yielding an experimental  $S_{BET}$  surface area of 1153  $m^2 g^{-1}$  (figs. S7 to S9).

Having confirmed that synthesis of im-COF-1 enabled formation of the targeted precursor framework encoded with cleavable olefinic bonds exclusively at the triangular pores, we next turned to the question of their cleavage. Our group and others have recently demonstrated that imine bonds can be broken in the presence of ozone (fig. S10) (35). Accordingly, we anticipated that this side reaction might hinder the orthogonal cleavage of olefinic bonds within the framework, thereby complicating the synthesis of our desired hexagonal macrocycles. Thus, we subjected im-COF-1 to a postsynthetic oxidation that first converted all the imine bonds into amide bonds, leading to a product (hereafter, am-COF-1) (36, 37) that we have demonstrated to be highly resistant to ozone (figs. S11 to S15). The oxidation entailed treating the iminic COF with sodium chlorite and acetic acid in the presence of 2-methyl-2-butene and dioxane (for the detailed synthetic protocol see the SM and fig. S16) (36).

The complete disappearance of the imine C=N stretching band (1620  $cm^{-1}$ ) and the subsequent appearance of the amide C=O stretching

<sup>1</sup>Catalan Institute of Nanoscience and Nanotechnology (ICN2), CSIC and The Barcelona Institute of Science and Technology, Campus UAB, Bellaterra, Barcelona, Spain. <sup>2</sup>Departament de Química, Universitat Autònoma de Barcelona (UAB), Cerdanyola del Vallès, Barcelona, Spain. <sup>3</sup>School of Engineering, Royal Melbourne Institute of Technology (RMIT), Melbourne, Australia. <sup>4</sup>Department of Chemistry and Kavli Energy Nano Sciences Institute, University of California, Berkeley, CA, USA. <sup>5</sup>Baker Institute of Digital Materials for the Planet, College of Computing, Data Science, and Society, University of California, Berkeley, CA, USA. <sup>6</sup>Institut de Química Computacional i Catalàlisi, Universitat de Girona, C/M. Aurèlia Capmany 69, Girona, Spain. <sup>7</sup>Servei de Resonància Magnètica Nuclear, Universitat Autònoma de Barcelona, Campus UAB, Bellaterra, Barcelona, Spain. <sup>8</sup>ICREA, Pg. Lluís Companys 23, Barcelona, Spain. <sup>9</sup>Institut de Ciència de Materials de Barcelona (ICMAB-CSIC), Bellaterra, Spain. \*Corresponding author. Email: jorge.albalad@icn2.cat (J.A.); inhar.imaz@icn2.cat (I.I.); daniel.masPOCH@icn2.cat (D.M.)

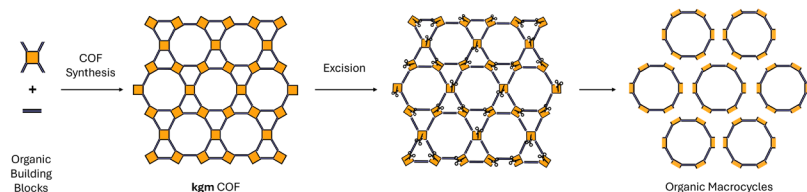


**Fig. 1. Schematic of the approach through excision of organic macrocycles from a COF.**

band ( $1656\text{ cm}^{-1}$ ) in the FTIR spectrum of am-COF-1 confirmed the successful oxidation of the imine to amide bonds (fig. S17). Additionally, the full conversion from imine to amide bonds was unambiguously confirmed by solid-state  $^{13}\text{C}$  CP-MAS NMR analysis (fig. S18), in which the carbon signals associated with imine groups ( $157.7\text{ ppm}$ ) gradually disappeared, as those corresponding to amide groups ( $166.5\text{ ppm}$ ) gradually appeared. Furthermore, the sharp and intense reflection at  $2.31^\circ$  in the PXRD pattern indicated that am-COF-1 retained the crystalline nature of the parent COF, without any appreciable changes to the long-range kgm topology (fig. S19).

### Synthesis of the polyamide-linked macrocycles

Having prepared am-COF-1, we next proceeded to cleave its olefinic bonds (Fig. 2A). We dispersed am-COF-1 in a mixture of *N,N*-dimethylformamide (DMF), tetrahydrofuran (THF) and methanol (MeOH), and the resulting dispersion was treated with ozone at a constant flow rate ( $30\text{ g N}^{-1}\text{ m}^{-3}$ ) at  $-78^\circ\text{C}$  for 10 minutes. The disconnection and liberation of discrete macrocyclic species became visibly apparent as the solid orange suspension transformed into a transparent yellow solution within the first 6 minutes (Fig. 2B). After ozonolysis, dimethyl sulfide (DMS) was added to the solution, which was stirred for 2 hours at room temperature to ensure total reductive ozonolysis—that is, the complete selective cleavage of all the olefinic bonds into aldehyde groups. The reaction mixture was then centrifuged to remove any solid traces, after which both THF and MeOH were removed from the supernatant. The remaining DMF solution was eluted through size-exclusion chromatography (BioBeads SX3, MW > 2000 Da). Addition of ethyl acetate (EtOAc) to the eluent led to precipitation of a crude solid. Finally, the crude product was washed with aqueous  $\text{Na}_2\text{CO}_3$ , water, and acetone, and then dried under high vacuum to obtain the desired macrocycle, comprising MC-1 functionalized with six aldehyde groups on its outer surface (hereafter, MC-1-CHO; yield: 90%; Fig. 2A, left). Notably, when performed on both a 10-mg and 1-g scale, this reaction maintained similar purities and yields (fig. S20). Electrospray mass spectrometry (ESI-MS) analysis of MC-1-CHO revealed a peak at  $[m/z] = 2531.7466$ , matching with the simulated isotopic distribution values attributed to the hexagonal macrocyclic species functionalized with six aldehyde groups (formula:  $[\text{C}_{162}\text{H}_{108}\text{N}_{12}\text{O}_{18} + \text{Na}]^+$ ; Fig. 2E and figs. S21 and S22).

We repeated the above synthetic protocol except under oxidative (rather than reductive) conditions to obtain MC-1 functionalized with six carboxylic acid groups (rather than aldehydes) on its outer surface (hereafter, MC-1-COOH; Fig. 2A, right). For this reaction, a dispersion of am-COF-1 in a mixture of DMF and THF was treated with ozone as described above. After ozonolysis, the reaction mixture was centrifuged to remove any remaining solid traces and the THF was removed from the supernatant. To ensure oxidative ozonolysis, Oxone was then added to the solution, which was stirred for 3 days at room temperature. Addition of water to the reaction mixture led to precipitation of a solid that was then washed with water and dissolved in DMF.

The resulting solution was eluted through size-exclusion chromatography (BioBeads SX3, MW > 2000 Da). Addition of water to the eluent led to precipitation of a crude solid. Finally, the crude product was washed with water and then dried under high vacuum to obtain MC-1-COOH (yield: 96%). Again, this oxidative reaction was successfully

performed at both 10-mg and 1-g scales (fig. S23). ESI-MS analysis of MC-1-COOH revealed a peak at  $[m/z] = 2627.7243$ , consistent with the simulated isotopic distribution values attributed to the hexagonal macrocyclic species functionalized with six carboxylic acid groups (formula:  $[\text{C}_{162}\text{H}_{108}\text{N}_{12}\text{O}_{24} + \text{Na}]^+$ ; Fig. 2F and figs. S24 and S25).

Once synthesized, we attempted to crystallize both macrocycles; however, all attempts were unsuccessful. Therefore, to gain further insight into the structures of MC-1-CHO and MC-1-COOH, we performed density functional theory (DFT) calculations to optimize the molecular geometries of both macrocycles (figs. S26 and S27). The DFT-optimized structures revealed that, once excised from the COF, the macrocycles are no longer planar. Instead, they adopt a distorted, twisted boat conformation due to torsional distortions around the amide bonds.

We further validated MC-1-CHO and MC-1-COOH in parallel by NMR spectroscopy, including  $^1\text{H}$  NMR,  $^{13}\text{C}$  NMR, heteronuclear single quantum coherence (HSQC), heteronuclear multiple bond coherence (HMBC), and diffusion-ordered spectroscopy (DOSY) experiments (DMSO- $d_6$ ), as well as by FTIR and elemental analysis (EA) (Fig. 2, C and D, and figs. S28 to S40). To facilitate interpretation of the NMR spectra, which exhibited broad and overlapping peaks, we synthesized three molecular models: Model-COF-1, which is analogous to the asymmetric unit of am-COF-1; and Model-CHO and Model-COOH, which are analogous to the repetitive 1/6th fragment of MC-1-CHO and MC-1-COOH, respectively (Fig. 2, C and D).

Briefly, Model-COF-1 was synthesized by reacting StTA with an excess of benzoyl chloride, yielding a soluble compound with an identical molecular structure to the COF precursor. Model-COF-1 was then subjected to ozonolysis under either reductive or oxidative conditions, affording the expected cleavage products, Model-CHO or Model-COOH, respectively, in quantitative yields (detailed protocol in the SM, and figs. S41 to S53). Comparing the  $^1\text{H}$  NMR spectra of the model molecules with those of the corresponding synthesized products corroborated that, upon each ozonolysis reaction, the olefinic bonds in am-COF-1 had been quantitatively cleaved, as evidenced by the complete disappearance of the singlet at  $7.73\text{ ppm}$  in both cases (Fig. 2, C and D). Under reductive conditions, a new aldehyde signal emerged at  $10.18\text{ ppm}$  (Model-CHO) and  $10.22\text{ ppm}$  (MC-1-CHO), integrating at a 1:2 ratio relative to the amide protons, which shift from  $10.36\text{ ppm}$  (Model-CHO) to  $10.65\text{ ppm}$  (MC-1-CHO). We ascribed these discrepancies to the differences in their respective electron delocalization.

Every aromatic signal in the model molecules was successfully assigned and matched with those observed in the macrocyclic species, except for the expected terminal protons (h,i) in Model-CHO (Fig. 2C), which are absent in the cyclic structure of MC-1-CHO. We observed a similar pattern for the reaction under oxidative conditions, with a broad peak at  $13.0\text{ ppm}$  appearing after complete cleavage of the alkene bond, which we attributed to formation of the carboxylic acid groups. Similarly, comparison of the  $^{13}\text{C}$  NMR spectra of the model molecules with those of the corresponding synthesized products enabled identification of every expected signal in the symmetric macrocyclic species (from  $\text{C}_2$  to  $\text{C}_{12}$ , fig. S54).

We observed two important differences: First, the spectra for Model-CHO and Model-COOH exhibited two additional signals ( $\text{C}_{13}$  and  $\text{C}_{14}$ ) that we attributed to terminal carbons and which are absent in the spectra for MC-1-CHO and MC-1-COOH. Second, the peak for the carbon that is alpha to the amide group ( $\text{C}_{11}$ ), located at  $136\text{ ppm}$  in the molecular models, shifted downfield ( $138\text{ ppm}$ ) because of the presence of symmetric amide bonds (in the *para*-position) throughout the macrocycle. Moreover, the small number of peaks in the 2D NMR analysis (HSQC, HMBC) of MC-1-CHO and of MC-1-COOH was consistent with highly symmetric closed species, as supported by good correlation between the  $^1\text{H}$ - $^1\text{H}$  and the  $^1\text{H}$ - $^{13}\text{C}$  couplings (figs. S30, S31, S36, and S37).

The DOSY analyses of MC-1-CHO and of MC-1-COOH revealed single diffusion-coefficients of *ca.*  $5.6 \cdot 10^{-11}\text{ m}^2\text{ s}^{-1}$  and  $6.5 \cdot 10^{-11}\text{ m}^2\text{ s}^{-1}$ ,

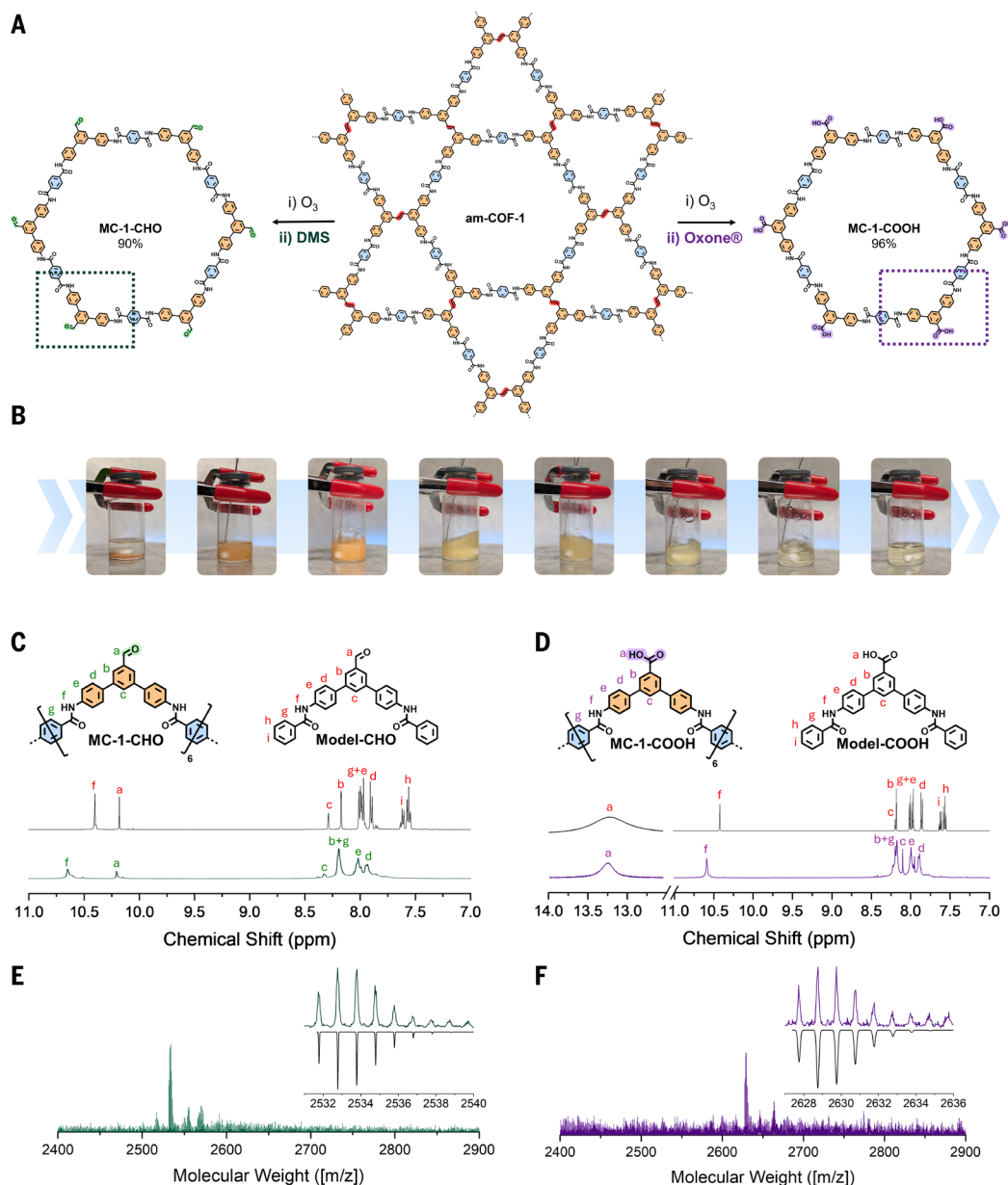


**Fig. 2. Overview of syntheses of MC-1-CHO and MC-1-COOH by selective ozonolytic cleavage of am-COF-1.** (A) Schematic of the syntheses under either reductive (MC-1-CHO) or oxidative (MC-1-COOH) conditions. The box highlights the repetitive units, which are used for <sup>1</sup>H NMR interpretation. (B) Photographs of the synthesis of MC-1-CHO through excision. (Left to right) Starting with a crystalline solid sample of am-COF-1 in a mixture of MeOH, DMF, and THF, ozone is bubbled into the dispersion, causing the cleavage of olefinic bonds and “dissolution” of am-COF-1 and release of macrocycles. Each image corresponds to a time lapse of ~1.5 min. (C and D) <sup>1</sup>H NMR spectra of MC-1-CHO (DMSO-d<sub>6</sub>, 500 MHz (C)) and of MC-1-COOH (DMSO-d<sub>6</sub>, 500 MHz (D)), as compared with those of Model-CHO and of Model-COOH, respectively. The region from 14.0 to 12.5 ppm is shown with increased intensity to highlight the presence of carboxylic acid protons. (E and F) ESI-QTOF MS spectra of MC-1-CHO (e, [m/z]: calculated for [C<sub>162</sub>H<sub>108</sub>N<sub>12</sub>O<sub>18</sub> + Na]<sup>+</sup> 2531.7797, found 2531.7466) and of MC-1-COOH (f, [m/z]: calculated for [C<sub>162</sub>H<sub>108</sub>N<sub>12</sub>O<sub>24</sub> + Na]<sup>+</sup> 2627.7492, found 2627.7243), with the corresponding comparison between experimental and simulated isotopic distribution.

respectively, corresponding to solvodynamic diameters in the ranges of 32.3 Å to 46.6 Å (MC-1-CHO), or 25.6 Å to 43.5 Å (MC-1-COOH). These values were consistent with the dimensions derived from DFT-optimized molecular structures of each macrocycle (figs. S26, S27, S32, and S38). The ensemble of analytical results unambiguously confirmed the formation of the targeted polyamide-linked macrocycles upon cleavage of olefinic bonds in the COF precursor, with chemoselective control of their peripheral functionality.

Finally, to further confirm the formation of the macrocycles and verify the accessibility of their external functional groups for postsynthetic modification, we covalently attached two different amine-terminated polyethylene glycol (PEG) chains (*ca.* 350 and 750 g mol<sup>-1</sup>) to each

of the six carboxylic acid groups of MC-1-COOH through amide bond formation. We hypothesized that the attachment of six PEG chains would significantly increase the molecular weight of MC-1-COOH, enabling clear detection of the functionalized macrocycles by Matrix-Assisted Laser Desorption/Ionization-Time of Flight (MALDI-TOF) mass spectrometry. Indeed, after postfunctionalization, MALDI-TOF analysis revealed a peak at (*m/z*) = 4777.9 for PEG<sub>350</sub> and at (*m/z*) = 6935.7 for PEG<sub>750</sub>, both consistent with the expected molecular weights of MC-1 functionalized with six PEG<sub>350</sub> and six PEG<sub>750</sub> chains, respectively (figs. S55 and S56).

As expected, the <sup>1</sup>H NMR spectra of both postfunctionalized macrocycles showed the disappearance of the broad peak at 13.0 ppm

attributed to the COOH groups, and the appearance of a signal at 8.81 ppm corresponding to the newly formed amides (figs. S55 and S56). PEG-related signals were observed at 3.50 ppm. The quantitative nature of the reaction was confirmed by the correct integration ratios: 90 aromatic protons from the central organic core, 18 amide NH protons, and approximately 192 PEG protons for PEG<sub>350</sub> or 428 for PEG<sub>750</sub>, consistent with the incorporation of six chains per macrocycle. Additionally, DOSY-NMR confirmed that all these signals belong to the same molecular species, with a diffusion coefficient of  $4.8 \times 10^{-11} \text{ m}^2 \text{ s}^{-1}$  in the case of the smaller PEG<sub>350</sub> chain and  $4.7 \times 10^{-11} \text{ m}^2 \text{ s}^{-1}$  for the larger PEG<sub>750</sub>-functionalized macrocycle (figs. S55 and S56).

### Design and synthesis of functionalized and large macrocycles

An advantage of using reticular materials such as COFs as precursors in this excision approach is that the well-established principles of reticular chemistry can be applied to rationally modify the precursor, thus enabling ready control over synthesis of new macrocycles (Fig. 3) (38, 39). For example, by using the isorecticular principle, we can substitute the linear dialdehyde PDA building block with one functionalized with fluorine groups, such as 2,3,5,6-tetrafluoroterephthalaldehyde (4F-PDA), to form a new COF (hereafter, am-COF-1-4F). Am-COF-1-4F is isostructural to am-COF-1 but has pores functionalized with fluorine atoms. We reasoned that because am-COF-1 ultimately led to MC-1, then am-COF-1-4F should afford fluoro-analogs of the macrocycles MC-1-CHO and MC-1-COOH (hereafter, MC-1-4F-CHO and MC-1-4F-COOH).

We further reasoned that we could apply the isorecticular expansion principle to rationally modify the sizes of the pores in the synthesized COFs. For example, we could substitute the linear dialdehyde PDA building block with larger ones, such as [1,1'-biphenyl]-4,4'-dicarbaldehyde (BPDA) or [1,1':4,1''-terphenyl]-4,4''-dicarboxaldehyde (TPDA), such that the synthesized COFs (hereafter, am-COF-2 and am-COF-3) would exhibit larger pores (inner cavity: 45.2 Å in am-COF-2 and 51.5 Å in am-COF-3 versus 35.3 Å in am-COF-1). This modification enabled synthesis of larger macrocycles, leading to MC-2 (a 138-atom ring macrocycle) and MC-3 (a 162-atom ring macrocycle).

Following the above strategy, we extended our excision approach to the synthesis of six additional macrocycles (Fig. 3). First, we synthesized am-COF-1-4F and am-COF-2, using a protocol similar to that used for am-COF-1. We confirmed the formation and purity of these COFs by PXRD, FTIR, <sup>13</sup>C CP-MAS NMR, and nitrogen physisorption studies (figs. S57 to S74). Next, we ozonized each COF using protocols similar to those used for MC-1-CHO and MC-1-COOH. This step afforded the fluoro-functionalized macrocycles MC-1-4F-CHO (yield: 90%) and MC-1-4F-COOH (yield: 92%), as well as the macrocycles MC-2-CHO (yield: 74%) and MC-2-COOH (yield: 86%), which are larger than their MC-1 counterparts.

We confirmed formation of these macrocycles by mass spectrometry [either ESI-quadrupole time-of-flight (QTOF) or MALDI-TOF], which revealed peaks corresponding to their molecular masses and isotopic distributions consistent with their formulas:  $[m/z] = 2963.5050$ , for MC-1-4F-CHO ( $[\text{C}_{162}\text{H}_{84}\text{F}_{24}\text{N}_{12}\text{O}_{18} + \text{Na}]^+$ );  $[m/z] = 3059.5208$ , for

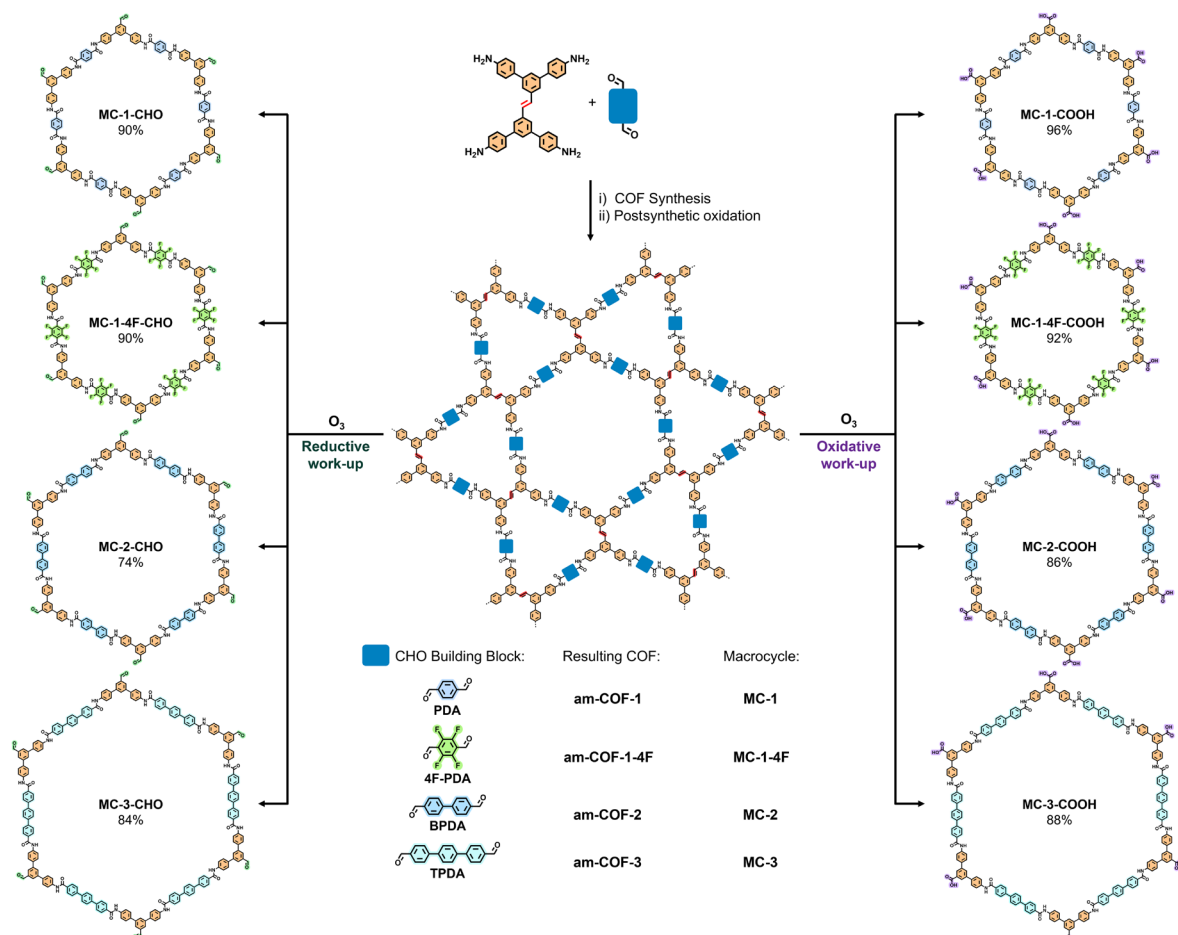


**Fig. 3. Isolation of isorecticular organic macrocycles.** Schematic showing the selective ozonolytic cleavage of olefinic bonds in each isorecticular COF liberates macrocycles, with precise control over the resultant functionalities, pore dimensions, and chemical environments.

MC-1-4F-COOH ( $[\text{C}_{162}\text{H}_{84}\text{F}_{24}\text{N}_{12}\text{O}_{24} + \text{Na}]^+$ ;  $[m/z] = 2987.9457$ , for MC-2-CHO ( $[\text{C}_{198}\text{H}_{132}\text{N}_{12}\text{O}_{18} + \text{Na}]^+$ ;  $[m/z] = 3061.9647$  for MC-2-COOH ( $[\text{C}_{198}\text{H}_{132}\text{N}_{12}\text{O}_{24} + \text{H}]^+$ ) (figs. S75 to S82). Finally, we validated formation of these four macrocycles by NMR spectroscopy, including by  $^1\text{H}$  NMR,  $^{13}\text{C}$  NMR, HSQC, HMBC, and DOSY experiments (DMSO- $d_6$ ), as well as by FTIR and EA (figs. S83 to S112).

The synthesis of MC-3-CHO and MC-3-COOH was performed with slightly modified protocols compared with those used for previous macrocycles because of their insolubility after cleavage from am-COF-3. After the synthesis of am-COF-3 (figs. S113 to S121), the product was dispersed in a mixture of DMF and THF (with MeOH also added for MC-3-CHO) and subjected to a constant ozone flow ( $30 \text{ g N}^{-1} \text{ m}^{-3}$ ) at  $-78^\circ\text{C}$  for 30 minutes. Subsequently, DMS or Oxone was added, and the mixture was stirred at room temperature for 2 hours and 6 days, respectively.

In both cases, the reactions proceeded in a solid-to-solid manner, attributed to the high insolubility of the large macrocycles. During the reaction, the orange-brown precursor gradually transformed into a pale-yellow product upon ozone exposure. The resulting products were washed sequentially with EtOAc, aqueous  $\text{Na}_2\text{CO}_3$ , water, and acetone for MC-3-CHO, and water and acetone for MC-3-COOH, before being dried under vacuum (yield: 84% for MC-3-CHO and 88% for MC-3-COOH). Despite their insolubility, both macrocycles were initially characterized by  $^1\text{H}$  NMR, using a minimal amount of solid dissolved in hot DMSO- $d_6$ . Notably, the resulting spectrum confirmed the formation of the respective macrocycle, displaying a profile similar to those of MC-1 and MC-2, with the expected 1:2 aldehyde-to-amide or carboxylic acid-to-amide ratios (figs. S122 and S125). Further characterization of both solids by quantitative deconvolution solid-state  $^{13}\text{C}$  NMR and FTIR spectroscopies also corroborated the macrocycle formation, consistently showing the same 1:2 aldehyde-to-amide or carboxylic acid-to-amide ratios (figs. S123, S124, S126, and S127).

## Synthesis to polyimide-linked macrocycles

Finally, to further demonstrate that our approach could synthesize other types of macrocycles, we applied it to synthesize one of the largest rigid polyimide macrocycles generated to date (40, 41). We began by synthesizing the precursor, which comprised a polyimide kgm COF (hereafter, pi-COF-1), in two steps: First, we synthesized a 2D iminic COF (im-COF-4), by reacting the alkyne-containing tetratopic  $\text{D}_{2h}$  linker 5,5''''-(ethyne-1,2-diyl)bis((1,1':3',1''-terphenyl)-4,4''-diamine)) (EBTD) with linear 2,5-dihydroxyterephthalaldehyde (2,5-OH-PDA) for 3 days at  $120^\circ\text{C}$ , using acetic acid as a catalyst and aniline as a modulator (detailed synthetic protocol in the SM, and figs. S128 to S134). Next, pi-COF-1 was synthesized through postsynthetic linker-exchange on the im-COF-4, using an excess of pyromellitic dianhydride at  $250^\circ\text{C}$  for 5 days, followed by an acid wash to remove any residual imine COF (fig. S135) (42, 43).

As confirmed by PXRD (fig. S136), the resulting pi-COF-1 ( $S_{\text{BET}} = 1934 \text{ m}^2 \text{ g}^{-1}$ , figs. S137 to S139) comprised a kgm framework, in which the hexagonal polyimide pores were interconnected by the bisection of the EBTD building block that contained a cleavable alkyne site. We chose alkyne bonds as a different cleavable bond option and one that exclusively yielded carboxylic acid products (44, 45). The complete exchange of imine moieties for imide bonds, forming the polyimide skeleton, was confirmed by FTIR (fig. S140). We observed the quantitative disappearance of the C=N stretching bands characteristic of imines ( $1613 \text{ cm}^{-1}$ ), and the appearance of the C=O stretching bands typical for imides ( $1723 \text{ cm}^{-1}$ ). Further validation by  $^{13}\text{C}$  solid-state NMR corroborated these findings, revealing a loss of the imine-C peak at 159 ppm and the emergence of a new imide-C peak at 165 ppm (fig. S141).

Next, we subjected pi-COF-1 to ozonolysis by first dispersing it in EtOAc and then exposing the resulting dispersion to a constant ozone flow ( $30 \text{ g N}^{-1} \text{ m}^{-3}$ ) with stirring for 40 minutes (Fig. 4A). Subsequently,

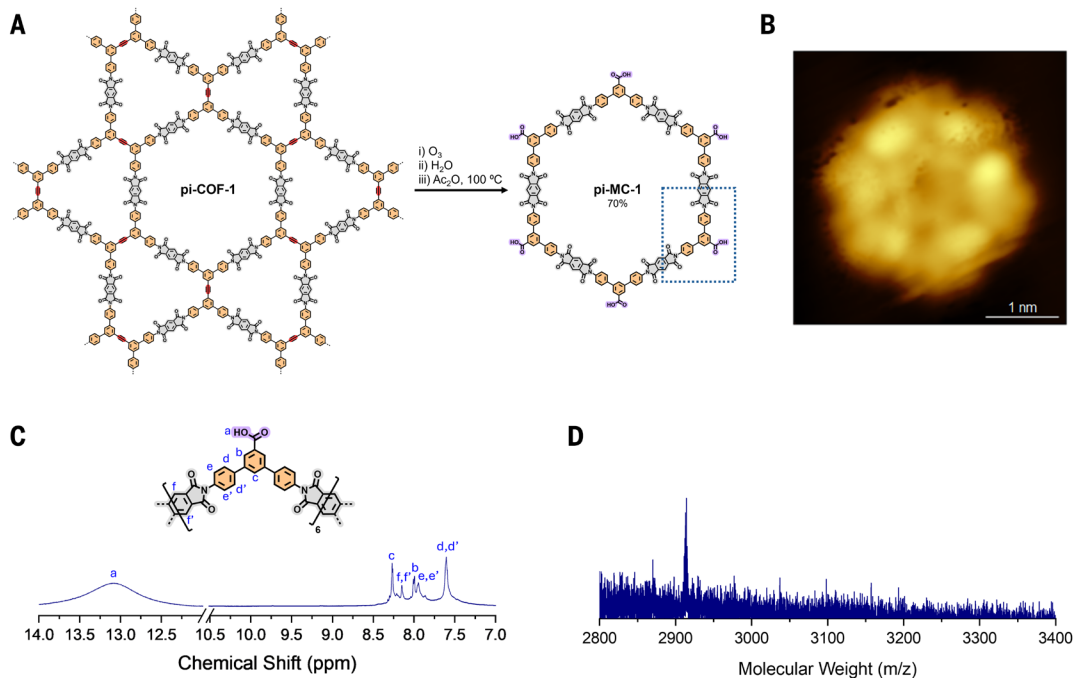


**Fig. 4. Overview of the synthesis of pi-MC-1 by selective ozonolytic cleavage of pi-COF-1.** (A) Schematic of the synthesis. (B) A representative STM image of a ring deposited on a Au(111) surface. Image size:  $3.8 \text{ nm} \times 3.8 \text{ nm}$ ; tunneling parameters:  $I_t = 500 \text{ pA}$ ,  $V_{\text{bias}} = 1.5 \text{ V}$ . Environmental conditions: deposition at  $T = 300 \text{ K}$ ,  $P < 5 \times 10^{-9} \text{ mbar}$ ; acquisition at  $T = 5 \text{ K}$ ,  $P < 1 \times 10^{-11} \text{ mbar}$ . (C)  $^1\text{H}$  NMR spectrum of pi-MC-1 (DMSO- $d_6$ , 500 MHz). The region from 14 to 12 ppm is shown with increased intensity to highlight the presence of carboxylic acid protons. (D) MALDI-TOF spectrum of pi-MC-1;  $[m/z]$ : calculated for  $[\text{C}_{174}\text{H}_{84}\text{N}_{12}\text{O}_{36}]^+$  2916.5111, found 2914.0335.

2 mL of water were added and the ozone flow was maintained for an additional 20 minutes. The resulting pale-yellow dispersion was filtered and the resultant solid was treated with acetic anhydride at 100 °C for 24 hours to prevent imide ring-opening, a reaction that is typically observed in discrete molecular imides (46). The product was then collected by centrifugation, dissolved in DMF, and eluted through size-exclusion chromatography (BioBeads MW > 2000 Da). It was precipitated out with EtOAc, isolated, and finally dried under dynamic vacuum to obtain the polyimide macrocycle (pi-MC-1) (yield: 70%) (Fig. 4A).

The formation of pi-MC-1 was first confirmed by MALDI-TOF mass spectrometry, which revealed a peak at  $[m/z] = 2914.0335$ , near the expected polyimide macrocyclic product containing six carboxylic acid groups at its external surface (calculated for  $[C_{174}H_{84}N_{12}O_{36}]^+$ ,  $[m/z] = 2916.5111$ , Fig. 4D and fig. S142). Next, the structure of pi-MC-1 was further validated by NMR spectroscopy, including  $^1H$  NMR (Fig. 4C),  $^{13}C$  NMR, HSQC, HMBC, and DOSY experiments (in DMSO- $d_6$ ), as well as by FTIR and EA (figs. S143 to S149).

Finally, we sublimated pi-MC-1 in ultrahigh vacuum conditions and deposited it on a Au(111) surface, which allowed us to visualize its structure using scanning tunneling microscopy (STM). Figure 4B shows the image of a ring (a larger-scale overview of the deposited rings can be found in fig. S150), further confirming its formation and detachment from the initial COF. The bright lobes and erratic spikes—the latter characteristic of dynamic effects—suggested a nonplanar (as confirmed by the torsional distortions of the DFT-optimized molecular structure of pi-MC-1, fig. S151), labile conformation that hindered atomic structural resolution. Nevertheless, the observed ring displayed the expected sixfold symmetry and a size matching the expected macrocyclic unit.

## Summary

In conclusion, we have introduced a synthetic approach for the design and preparation of organic macrocycles through their excision from COFs. This method relies on the spontaneous formation of macrocycles during assembly of COFs, in which some of the pores are delineated by the macrocycles themselves. Initially, reticular chemistry was used to design and construct the COF, incorporating repeated units of the target macrocycle separated by cleavable bonds such as double or triple bonds. Subsequently, the COF was subjected to a cleavage reaction—in the case we have reported here, ozonolysis—to liberate the macrocycles, thus enabling their synthesis with precise selectivity control and high yields. Notably, the choice of reductive or oxidative conditions for the ozonolysis dictated the functional groups, either aldehyde or carboxylic acid groups, that appear at the external surface of the macrocycle. We have demonstrated the versatility of our approach by synthesizing nine macrocycles of distinct skeletal composition (based on polyamide and polyimide linkages), functionalities, and/or sizes. Given the wide variety of repetitive (macro)molecules such as cages, catenanes, and polymers that can be spontaneously formed within the COFs during assembly, we believe that our approach could provide generalized access to previously inaccessible (macro)molecules and polymers at the molecular level, including structurally sophisticated macrocycles, for diverse applications.

## REFERENCES AND NOTES

- K. C. Nicolaou, J. S. Chen, *Chem. Soc. Rev.* **38**, 2993–3009 (2009).
- J. Li, M. D. Eastgate, *Org. Biomol. Chem.* **13**, 7164–7176 (2015).
- S. V. Rosokha, J. K. Kochi, *J. Org. Chem.* **67**, 1727–1737 (2002).
- C. Chen *et al.*, *J. Am. Chem. Soc.* **142**, 1332–1340 (2020).
- C. C. Chintawar, A. K. Yadav, A. Kumar, S. P. Sancheti, N. T. Patil, *Chem. Rev.* **121**, 8478–8558 (2021).
- J. F. Lutz, M. Ouchi, D. R. Liu, M. Sawamoto, *Science* **341**, 1238149 (2013).
- A. Ya-Ting Huang, C. L. Kao, A. Selvaraj, L. Peng, *Mater. Today Chem.* **27**, 101285 (2023).
- O. M. Yaghi, M. J. Scott, R. H. Holm, *Inorg. Chem.* **31**, 4778–4784 (1992).
- Y. Yang *et al.*, *Angew. Chem. Int. Ed.* **61**, e202111228 (2022).
- S. Ruiz-Relaño *et al.*, *J. Am. Chem. Soc.* **146**, 26603–26608 (2024).
- D. Nam *et al.*, *J. Am. Chem. Soc.* **146**, 27255–27261 (2024).
- Y. Itoh *et al.*, *Science* **376**, 738–743 (2022).
- X. N. Han, Y. Han, C. F. Chen, *Chem. Soc. Rev.* **52**, 3265–3298 (2023).
- V. Martí-Centelles, M. D. Pandey, M. I. Burguete, S. V. Luis, *Chem. Rev.* **115**, 8736–8834 (2015).
- K. Katagiri, T. Tohaya, H. Masu, M. Tominaga, I. Azumaya, *J. Org. Chem.* **74**, 2804–2810 (2009).
- H. M. Colquhoun *et al.*, *Chemistry* **16**, 907–918 (2010).
- Y. Wang, H. Wu, J. F. Stoddart, *Acc. Chem. Res.* **54**, 2027–2039 (2021).
- D. G. Hamilton, L. Prodi, N. Feeder, J. K. M. Sanders, *J. Chem. Soc., Perkin Trans. 1* **1**, 1057–1066 (1999).
- F. Zeng, L.-L. Tang, M.-H. Ding, W. Dessie, *Org. Lett.* **25**, 6290–6294 (2023).
- K. Nakao *et al.*, *J. Am. Chem. Soc.* **128**, 16740–16747 (2006).
- Y. Y. Zhu, C. Li, G. Y. Li, X. K. Jiang, Z. T. Li, *J. Org. Chem.* **73**, 1745–1751 (2008).
- A. P. Côté *et al.*, *Science* **310**, 1166–1170 (2005).
- C. S. Diercks, O. M. Yaghi, *Science* **355**, eaal1585 (2017).
- K. Geng *et al.*, *Chem. Rev.* **120**, 8814–8933 (2020).
- F. Haase, B. V. Lotsch, *Chem. Soc. Rev.* **49**, 8469–8500 (2020).
- T. Prakasam *et al.*, *Chem* **11**, 102307 (2025).
- Y. Liu *et al.*, *Science* **351**, 365–369 (2016).
- X. Han *et al.*, *J. Am. Chem. Soc.* **145**, 22885–22889 (2023).
- F. Chen *et al.*, *Chem. Soc. Rev.* **54**, 484–514 (2025).
- Y. Tian *et al.*, *CrystEngComm* **19**, 4877–4881 (2017).
- J. Tu, W. Song, B. Chen, Y. Li, L. Chen, *Chemistry* **29**, e202302380 (2023).
- J. Li *et al.*, *Chem. Commun.* **59**, 13191–13194 (2023).
- Y. Wang *et al.*, *ACS Mater. Lett.* **6**, 140–152 (2024).
- A. Natraj *et al.*, *J. Am. Chem. Soc.* **144**, 19813–19824 (2022).
- D. Yan, Z. Wang, P. Cheng, Y. Chen, Z. Zhang, *Angew. Chem. Int. Ed.* **60**, 6055–6060 (2021).
- P. J. Waller *et al.*, *J. Am. Chem. Soc.* **138**, 15519–15522 (2016).
- Z.-B. Zhou *et al.*, *J. Am. Chem. Soc.* **144**, 1138–1143 (2022).
- W. Li *et al.*, *Adv. Funct. Mater.* **32**, 2207394 (2022).
- Z. Mu *et al.*, *J. Am. Chem. Soc.* **144**, 5145–5154 (2022).
- P. Spenst *et al.*, *J. Am. Chem. Soc.* **139**, 2014–2021 (2017).
- T. Iwanaga *et al.*, *Angew. Chem. Int. Ed.* **45**, 3643–3647 (2006).
- J. Maschita, T. Banerjee, B. V. Lotsch, *Chem. Mater.* **34**, 2249–2258 (2022).
- M. K. Shehab, K. S. Weeraratne, O. M. El-Kadri, V. K. Yadavalli, H. M. El-Kaderi, *Macromol. Rapid Commun.* **44**, e2200782 (2023).
- D. J. Miller, T. E. Nemo, L. A. Hull, *J. Org. Chem.* **40**, 2675–2678 (1975).
- N. Havare, *ARKIVOC* **2023**, 202211942 (2023).
- S. V. Vinogradova *et al.*, *Polymer Sci. USSR* **16**, 584–589 (1974).

## ACKNOWLEDGMENTS

We extend our gratitude to L. Gómez and V. Oliveras from the Serveis Tècnics de Recerca at the University of Girona (STR-UdG) and N. Cabello from the High-resolution Mass Spectrometry Unit at the Institut Català d'Investigació Química (ICIQ) for their invaluable insights and continuous support in conducting mass spectrometry measurements throughout the project. We also thank H. Celik, R. Giovine, and the Pines Magnetic Resonance Center's Core NMR Facility (PMRC Core) for spectroscopic assistance. The instrument used in this work is supported by the National Science Foundation under grant 2018784. We thank CESA Supercomputing Center for technical support and computer time at the supercomputer FinisTerra III. **Funding:** This work has received funding from the European Union's Horizon 2020 research and innovation program under grant agreement 101019003, grant ref PID2021-124804NB-I00 and PID2022-136970NB-I00 funded by MCIN/AEI/10.13039/501100011033/ and by "ERDF A way of making Europe", and the Catalan AGAUR (project 2021 SGR 00458, project 2021 SGR 01519, and project 2021 SGR 00475). It was also funded by the CERCA program/Generalitat de Catalunya. ICN2 and ICMA are supported by the Ochoa Centres of Excellence programme, grants CEX2021-001214-S and CEX2023-001263-S, funded by MCIN/AEI/10.13039/501100011033 and by FEDER, the European Union (EU). J.P.C. is grateful for his PhD grant, funded from the Marie-Sklodowska Curie grant agreement 101034328. S.F. acknowledges the grant agreement 101149783 - ATOSENSE funded by the European Union. This paper reflects only the authors' views, and the Research Executive Agency is not responsible for any use that may be made of the information it contains. C.F.E. is grateful for a Beatrú de Pinós contract (2022–BP–0078). X.R. is grateful for an ICREA Acadèmia award. **Author contributions:** Conceptualization: J.A., O.M.Y., I.I., and D.M.; Funding acquisition: D.M. Investigation: R.S.N., J.P.C., J.A., A.C.M., K.W., S.F., and E.R. Methodology: R.S.N., J.P.C., J.A., A.C.M., K.W., T.P., C.F.E., X.R., and A.M. DFT calculations: J.F. Supervision: J.A., O.M.Y., I.I., and D.M. Writing – original draft: R.S.N., J.P.C., and J.A. Writing – review & editing: J.A., O.M.Y., I.I., and D.M. **Competing interests:** ICN2, ICREA, and CSIC have applied for a patent on the synthesis of macrocycles via Clip-off Chemistry, on which D.M., I.I., J.A., R.S.N., and J.P.C. are listed as co-inventors. **Data and materials availability:** All data are available in the main text or the supplementary materials. All isotherm data in adsorption information file format (.aif); the XYZ files, including the coordinates of the DFT geometry optimization files, are available as digital files in the supplementary materials. **License information:** Copyright © 2025 the authors, some rights reserved; exclusive licensee American Association for the Advancement of Science. No claim to original US government works. <https://www.science.org/about/science-licenses-journal-article-reuse>

## SUPPLEMENTARY MATERIALS

science.org/doi/10.1126/science.adw4126  
Materials and Methods; Figs. S1 to S151; Table S1; References (47–64)  
Submitted 1 February 2025; accepted 16 April 2025

10.1126/science.adw4126